Towards Automated Robot-Based Nanohandling

Fatikow S., Wortmann T., Mikczinski M., Dahmen C., Stolle C.
Division Microrobotics and Control Engineering (AMiR), University of Oldenburg, Germany
E-mail: fatikow@uni-oldenburg.de

Abstract: One of the key challenges of microsystem- and nanotechnologies is the automation of robot-based nanomanipulation. However, there is limited sensor feedback due to lack of appropriate sensors. Sensor feedback is required for repeatable actuator movements from macro- down to the nanoscale. This complicates the design of reliable automation processes. In this paper, the development of an automated robot-based toolbox for cell injection and handling is presented. This toolbox includes several sensor methods, bridging several orders of magnitude as feedback for automation. A non-linear support vector machine (SVM) is applied for classification of the viability of cells as feedback for quality control. A visual servoing algorithm for position tracking of the injection needle as well as an injection force sensor have been developed. First automation results and the control system are explained.

Key Words: Nanohandling, cell classification, visual servoing, force-sensing, distributed control architecture

1 INTRODUCTION

Over the last decade, there has been an increasing interest on the automation of manipulation, handling, and assembly tasks on the micro- and nanoscale [1]. A key constraint of automated nanohandling is the very limited sensor feedback due to the required resolutions and the small type of construction of nanorobots. Therefore, existing techniques need to be scaled down if feasible or new sensor methods need to be developed.

In the project "Hybrid ultra precision manufacturing process based on positional- and self-assembly for complex micro-products" – HYDROMEL [2], the goal is to develop tomorrow's high-precision flexible and cost-effective manufacturing process for complex microproducts. This goal should be achieved by combining self-assembly [3] and nanorobotic techniques [4]. This paper will focus on the sensor and control concept of a flexible high-throughput cell injection system demonstration, which is part of HYDROMEL.

The automated injection of Xenopus Laevis oocytes (African clawed frog) has been chosen as application for the developed algorithms and sensors. The injection process, though actually happening on the microscale, shows all characteristics of a similar handling process on the nanoscale. The components – except the force sensor – which are needed for nanohandling will differ just in details.

In order to enable a successful injection process, different components are needed. The first step is the sorting of the oocyte cells according to their suitability for injection. Defective cells should not be injected but rejected by the system and disposed. For this purpose, a cell classification algorithm has been developed (section 2). After this prescreening, the cells have to be injected. A needle tip tracking algorithm is used to obtain feedback about the tip position, and visual servoing is therefore executed to position the needle relative to the cell (section 3). When the needle is ready to inject, force feedback delivers information about the contact forces between cell and needle tip, by which the injection process can be monitored and validated (section 4). Finally, a control system architecture integrating the different sensor feedback methods of the previous sections is presented in section 5.

This work was part funded by the European Commission FP6 Integrated Project HYDROMEL.

2 CELL CLASSIFICATION

Automatic microinjection of biological cells is considered to be a key technology in biotechnological research. Especially in drug development, the Xenopus Laevis is a very popular model organism because of its rapid growth. Also oocytes and embryos are comparably robust to manipulations. For automated microinjection of Xenopus Laevis oocytes, the quality of the raw cells must be controlled to assure reproducible results. Usually, the oocytes are separated manually from the frog so defects such as incomplete separation, external damage or oocyte death may occur.

The characterization of biological cells from a streaming cell suspension is referred to as flow cytometry [5]. Traditionally, laser scatter is used to derive several parameters from thousands of cells per minute. This technique is used for cells of up to a few hundred microns in diameter whereas the oocytes considered here are around 1 mm, depending on maturation state. An approach more promising is image cytometry [6]. In image cytometry cell properties are measured from microscopic images. This procedure exhibits many details of individual cells but comes with the drawback of limited throughput.

An experimental setup has been built for automatic oocyte classification based on image cytometry. The cells travel along a microfluidic channel passing the field of view (FOV) of a programmable camera module (Videology 21K15X) which provides a video stream to the computer

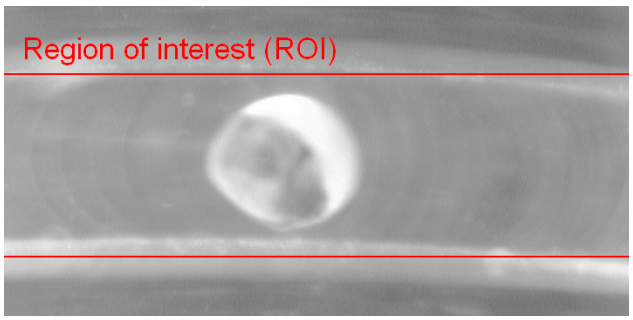

Figure 1: Image scene of a viable Xenopus Laevis oocyte in motion with marked region of interest (ROI).

vision application. This setup allows for classification of oocytes in real-time. If an object is detected, the computer vision application indicates the classification result to the process controller which will remove the object if necessary. A typical image scene containing a viable oocyte can be seen in figure 1.

2.1 Segmentation

For obtaining relevant features from a cell image, objects have to be separated from the image background. This procedure is called image segmentation. If constant illumination is ensured during the experiments a raw segmented image may be received by calculating the absolute difference of the actual image and an initially captured background image. The Canny Edge Detector [7] applied to the difference image helps to find the outer and inner contours of the cell. Finally, binary dilation applied to the edge image followed by region filling yields a segmentation mask. This binary mask indicates oocyte and background regions of the original image.

2.2 Feature Retrieval

Four damaged and dead oocytes can be seen in figure 2. Once an object enters the FOV three features are computed that serve as input to the classifier.

1. Object size obtained by the number of object pixels
2. Object roundness R as described in [8]:

$$R = \frac{4\pi \cdot Area}{Perimeter^2} \tag{1}$$

3. Average textural contrast as described in [9]

The size feature ensures that cell debris that might result from cell damage cannot be classified as viable cell. Defects in object roundness R are a sign of cell surface burst. A neighborhood of 5 pixels has been chosen for the average textural contrast feature. Higher values correspond to a high level of cell pigmentation which is an indicator for cell death. All features are normalized before classification.

2.3 Classification and Results

A non-linear SVM approach has been chosen for classification using SVM^{light} software [10]. The training procedure includes 212 representative samples and identifies 37 support vectors s_i with associated Lagrange multipliers α_i and hyperplane threshold b. The radial basis function (RBF) kernel is used as non-linear feature mapping:

$$K\left(\mathbf{x_i}, \mathbf{x_j}\right) = e^{-||\mathbf{x_i}-\mathbf{x_j}||^2} \tag{2}$$

Leave-one-out cross validation indicates an error of 0.0189. The classification is performed online according to the rule:

$$f\left(\mathbf{x}\right) = \sum_{i=1}^{N_s} \alpha_i y_i K\left(s_i, \mathbf{x}\right) + b \tag{3}$$

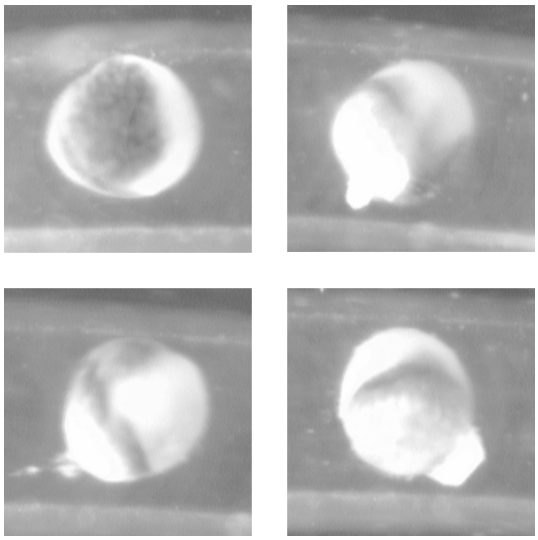

Figure 2: Four examples of damaged and dead oocytes.

3 VISUAL SERVOING

One task in the HYDROMEL project is to automatically inject substances into oocyte cells. For this, an injection setup is being developed to achieve high throughput of cells in combination with high injection success rate and precision.

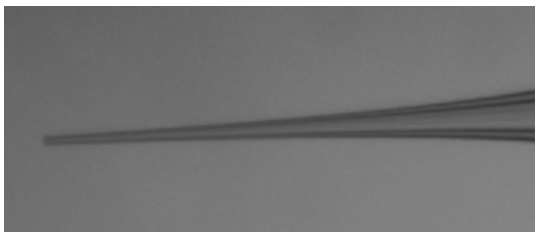

Figure 3: Example for injection needle used in setup.

In order to control the injection process for the Xenopus Laevis oocytes, the injection needle position has to be tracked. The method used for this purpose is based on template matching. With the position data of the tracking algorithm, the needle can be moved to the cell of interest by visual servoing. Using visual tracking for this purpose enables the injection station to flexibly adjust to different cell positions and setup changes.

The template matching approach uses normalized cross correlation to locate a known object in a scene. A template image T containing the object of interest is cross correlated with the camera input image I:

$$C(x_p, y_p) = \sum_{x=0}^{x_t} \sum_{y=0}^{y_t} I(x_p + x, y_p + y) \cdot T(x, y) \quad (4)$$

The position of the maximum in this cross correlation matrix is the position of the object in the image:

$$C(x_{object}, y_{object}) = max(C) \quad (5)$$

To further refine the object's position in the image, the correlation matrix is constrained with a suitable threshold function:

$$T(v) = \begin{cases} v - t & \text{if } v >= t \\ 0 & \text{else.} \end{cases} \quad (6)$$

$$C_{thresh}(x, y) = T(C(x, y)) \quad (7)$$

and subsequently a weighted centroid is calculated of the area surrounding the object's position:

$$x_{cog} = \frac{\sum x \cdot C(x, y)}{\sum C(x, y)} \quad (8)$$

$$y_{cog} = \frac{\sum y \cdot C(x, y)}{\sum C(x, y)} \quad (9)$$

By using this approach, the position of the needle tip can be determined to fractions of a pixel.

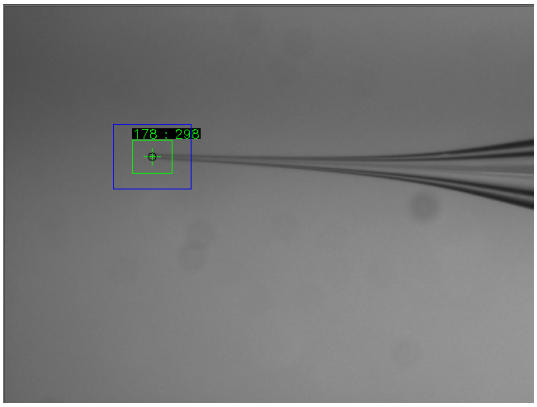

Figure 4: Injection needle tracked using template matching.

Problems may occur if the needle tip is leaving the focal plane of the camera. Small displacements already lead to increasing defocusing. To a certain point, the template matching approach is robust against defocusing, but the robustness is limited by the appearance of the object. Due to the small dimensions of the tip in the image, a certain amount of defocusing may lead to the tip appearing shorter than it is. This will alter the tracked tip position.
This approach is not restricted to light microscope images. Another possible application of it is the tracking of nanometer-sized objects (figure 5) in the scanning electron microscope (SEM). The specific imaging constraint of the SEM is the poor signal to noise ratio when using fast scanning speeds. The template matching approach is robust against this increased level of noise, so it can be used in a nanohandling setup with SEM as visual sensor. Defocusing issues on the other hand are not evident to the same extent.

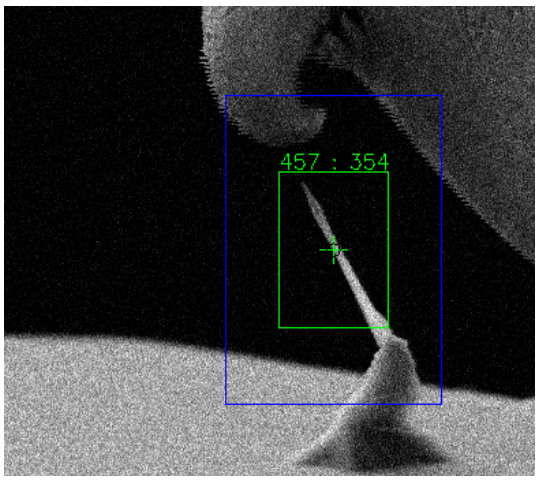

Figure 5: Nanowire tracked using template matching.

The implementation of the template matching algorithm is efficient enough to process camera images in real-time for common image sizes and frame rates, due to the restriction of the algorithm to a search area around the last determined position of the object.
Tests have shown that the tracking algorithm is working stable and fast for this setup and for manipulation setups in the nanometer scale. Further miniaturization of the setup will be possible using this approach.

4 FORCE SENSORS

Forces play a major role in ones everyday life and especially regarding actions on the micro- to nano-scale. In the special case of handling living cells, it is important to limit the forces acting on the cells by the tools. Cell handling tools are for example grippers [11], patch-clamp pipettes, and injection pipettes.
Regarding a tele-operation or even an automation of the injection process, the injection force is an indispensable factor. At the moment, in nearly all laboratories, the injection is still done by hand. The operator relies on his or her skills and experience and the number of successful injected cells is rather low [12]. The bottle-neck is the force measurement. Forces can be measured by optical means but this requires additional computing resources and rely on deformable objects [13][14]. Here, a mechanical force sensor would be beneficial as with an appropriate method the sensor uses fewer resources and makes a direct contact instead of optical methods.
We are developing such a sensor intended e.g. to measure the injection forces during the injection of the above mentioned Xenopus Laevis oocytes.

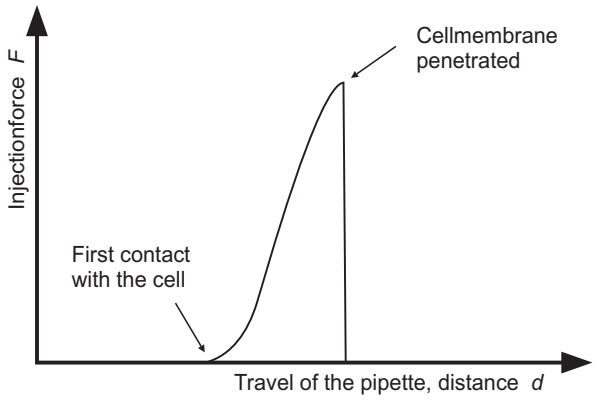

Figure 6: Typical force-distance curve for an injection of a cell in general (compare [15],[16]).

A typical force-distance curve of a cell injection (figure 6), starts with no or just a low force as there is no contact with any cell, but with the medium in which the oocytes live. When the pipette is touching a cell, the force is rising until the cell membrane is penetrated. With the penetration, the forces on the pipette drop down to another minimum. The force differences during the individual injection states are significant and a proper force sensor will be able to resolve them properly for an automation system.

For different cell types, one can find different values of forces in literature. For example, penetration forces of mouse embryos and mouse oocytes are about 13 μN and 7.5 μN [17], respectively, or Drosphelia embryos are about 50 μN [18], or zebrafish embryos are about several hundreds of micronewtons [16] (ca. 700 μN, [14]). However, from these values, we estimate the force range for the injection of the bigger Xenopus oocytes from several hundreds of micronewtons up to not more than five millinewtons.

As there is no way to measure forces directly, a structure to transform the force has to be used. Our approach is to use a cantilever structure which transforms the acting force into stress and strain, similar to those in [19]. The strain can be detected with strain gages. A possible structure can be seen in figure 7. The concentration of stress can be plainly seen in the model.

As for strain gages, the strain is mandatory an approximation is done. Cutting the sensor clear, we get a typical cantilever beam and can derive the strain ϵ from the known beam bending equation:

$$\epsilon = \frac{6 \cdot l}{E \cdot w \cdot h^2} \cdot F \tag{10}$$

with the acting force F, the active length l of the cantilever (analogous to optics: projected length), Young's Modulus E, width w, and height h of the beam. Assuming 1 mN as acting force and the transducer disc made from steel with $E = 200\ kN/mm^2$ and dimensions of $h = 0.2\ mm$ and $w = 0.3\ mm$ and the active length of one clear-cut beam $l = 3.6\ mm$ we determine the strain to $\epsilon = 4.5\ \mu m/m$. The maximum allowable strain is given

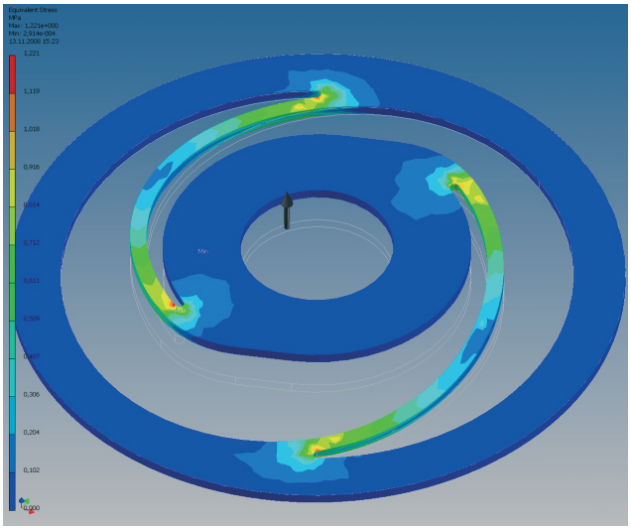

Figure 7: CAD-model of the sensor design. A preliminary simulation with an acting force of 1 mN was done showing stress in the range from zero (blue) to 1.2 N/mm^2 (red, color online).

with 3000 $\mu m/m$ for the intended strain gages KSN-2-120-E5-16 (from KYOWA, Japan).

On the sensor, we can implement two full Wheatstone bridges - one on every beam. As the strain on both ends of the beam is equal we can approximate the resulting voltage of a whole Wheatstone bridge for the calculated strain. Using the known equation:

$$U_{bridge} = U_{supply} \cdot k \cdot \epsilon \tag{11}$$

with the supply and bridge voltages $U_{supply} = 2.5\ V$ and U_{bridge}, respectively, the strain gage specific gage factor $k = -110$, and the above calculated strain ϵ, the result of this equation is $U_{bridge} = -1.24\ mV$.

For the following signal processing, the signals need to be amplified. The equal change in both signals gives the elongation of the sensor. Differences are a hint on side effects and non-axial forces.

Obviously, this setup will make it possible to detect injection forces as small as 1 mN. The resulting strain is far from the strain gages limit. Even with an assumed preloading of $3g$ (by the pipette and holding parts) the strain rises just up to approximately $137 \mu m/m$. A mechanical setup to hold the sensor and connect pipette and tubing is also under construction. For sensor testing a patch-clamp system is available to hold the cell. In the later project setup the cells are immobilized in a vacuum-based device.

The automation of an injection-system or -robot depends not just on the positioning system but also on the force sensor. Therefore, more efforts have to be spent designing an appropriate sensor. The signal from the force sensor will enable researchers to do the injection teleoperated with force feedback [15] or enable micro- or nanorobots to do the injection automatically. This will boost the positive injection results and the overall throughput of the injection system.

5 CONTROL ARCHITECTURE AND AUTOMATION

5.1 Control Architecture

The methods and algorithms presented for force measurement, pattern recognition and visual servoing provide a sensor toolbox for a reliable cell injection automation process. These techniques need to be integrated into a common software architecture. The distributed control architecture for automated nanohandling (DCAAN) [20] has been chosen for this task. It is a flexible Common Object Request Broker Architecture (CORBA) based control system, which is capable of integrating sensor and low-level control programs into one common framework. As first step towards integration all components of the toolbox have been included into the network structure (see Figure 8).

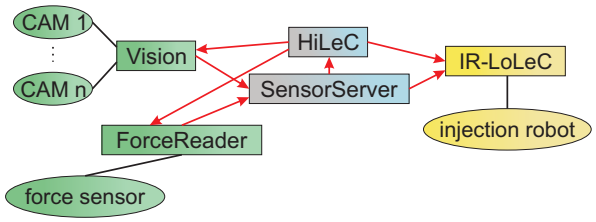

Figure 8: The control architecture includes force and visual sensors. The different servers (rectangles) are connected via CORBA (red arrows).

Vision processes all camera input. Tracking and classification algorithms (see sections 2 and 3) are applied in Vision and their result is sent to SensorServer. Sensor programs such as Vision send the current sensor data to SensorServer. The SensorServer program acts as a data hub. It distributes the sensor data to all servers that require this input (e.g. low-level controllers). The force sensor readings are processed by the ForceReader server and the injection robot is controlled by the low-level controller IR-LoLeC. The high-level controller (HiLeC) is responsible for the execution of automation sequences as well as for user input handling.

5.2 Script Language for Automation Sequences

The automation of nanohandling tasks has very high demands on the automation language. Automation scripts combine process primitives (e.g. movement commands) of sensor programs and LoLeCs. Every DCAAN component specifies its own process primitives as a list of commands, parameters and return types. Hence, new commands provided by servers can be integrated quite easily into automation scripts. The commands have the structure:

```
<comp>.<prim>(<param>*<res>*),
```

where *comp* is the server component (e.g. vision), *prim* is the name of the process primitive with a set of paramters (*param*) and a set of result values (*res*). Examples for process primitives are *MoveClosedLoop*, *ActivateCamera* and *GetForceReading*. The automation sequences themselves are written in the scripting language Python, which makes HiLeC automation problems independent. Parallel control cycles are modeled as python threads. For new hardware setups, only the automation sequences need to be adapted to the new server dependent command sets. Error handling can be performed on user level.

5.3 Injection control

The cell classification and the cell injection need to run in parallel to ensure the high throughput constraints. Therefore, the injection process is automated using three control cycles (see Figure 9). One control cycle (dashed arrows on the left hand side) is for the force controlled injection process. The ForceReader evaluates the current sensor signal and sends the resulting value to the SensorServer program. The movement velocity of the injection robot is adapted by IR-LoLeC dependent on the current force measurement.

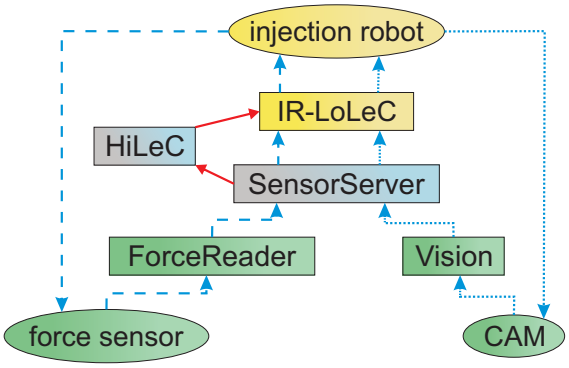

Figure 9: Control cycles of the automated cell injection system.

The second control cycle (dotted arrows on the right hand side) controls the position of the injection needle. The camera images are processed by Vision and sent to the SensorServer. This position data is read by the IR-LoLeC to calculate the error vector with respect to the current position and the goal position. Low-level actuation signals are generated according to this error vector. The last control cycle uses the same path as the second cycle. It is used for the cell classification algorithm. Dependent on the classification decision, the defect cells just pass the injection station without injection.

The automation sequences in HiLeC build a meta control cycle. Movement commands are sent to IR-LoLeC dependent on the position reading, the viability feedback of the cell and the current force measurement are used as control feedback. The sequence distinguishes four different states. If there is no cell in the field of view the needle is moved into a predefined save position. The same happens if there is a defect cell. The second and the third states depend on the force reading and the distance between needle and the viable cell. If there is no force reading, the needle is moved using the second control cycle. The force reading is used for velocity control (first control cycle) as soon as a contact between needle and cell membrane is detected by the force sensor. At the time the membrane is penetrated, the force value decreases rapidly. In the last state, the needle

is moved to the final injection position utilizing the radius information of the cell and the current positions.

6 CONCLUSION

In this paper, several key components for an automated robot-based cell injection system have been presented. They are crucial for the high throughput required for a future manufacturing system with low error rates. The separate components are suitable for integration into the overall setup.

An SVM-based algorithm to evaluate the viability of cells for quality control has been introduced. The required control feedback for an automated injection process has been proposed. This feedback consists of a template-based visual servoing method for position tracking and a force sensor to monitor the forces during the injection process. The algorithms have been applied to Xenopus Laevis oocytes cells. The applicability of these components and algorithms has been illustrated and the possible use of some of these for the automation of handling processes on an even smaller scale has been discussed.

More experiments with different cell types need to be performed to ensure generalization ability of the quality control algorithm and the force-sensor. The next steps are the integration of these components into an appropriate micro fluidic setup and the evaluation of the overall performance.

7 ACKNOWLEDGEMENTS

This work was partly funded by the European Commission FP6 Integrated Project HYDROMEL. The authors would like to thank all partners involved into the project for the great cooperation.

REFERENCES

[1] C. Clevy, A. Hubert, and Chaillet N., "Micromanipulation and Micro-Assembly Systems," *The IARP - IEEE/RAS - EURON Joint Workshop on MICRO & NANO ROBOTICS (av. online at: http://iarp06.robot.jussieu.fr/)*, 2006.

[2] "Hydromel - hybrid ultra precision manufacturing process based on positional- and self-assembly for complex micro-products." [Online]. Available: http://www.hydromel-project.eu

[3] G. M. Whitesides and B. Grzybowski, "Self-assembly at all scales." *Science*, vol. 295, no. 5564, pp. 2418–2421, March 2002. [Online]. Available: http://dx.doi.org/10.1126/science.1070821

[4] S. Fatikow, T. Wich, H. Hlsen, T. Sievers, and M. Jhnisch, "Microrobot system for automatic nanohandling inside a scanning electron microscope," in *Proc. of Int. Conference on Robotics and Automation (ICRA'06)*, Orlando, FL, U.S.A., May 2006, pp. 1402–1407.

[5] L. Bonetta, "Flow cytometry smaller and better," *Nature methods*, 2005.

[6] C. Waehlby, "Algorithms for applied digital image cytometry," Ph.D. dissertation, Uppsala University, Centre for Image Analysis, 2003.

[7] R. C. Gonzalez and R. E. Woods, *Digital Image Processing*. Addison-Wesley, 1992.

[8] M. L. Hentschel and N. W. Page, "Selection of descriptors for particle shape characterization," *Particle & Particle Systems Characterization*, 2002.

[9] R. Haralick, "Textural features for image classification," in *IEEE Trans. on Systems, Man and Cybernetics*, 1973.

[10] T. Joachims, "Making large-scale svm learning practical," *Advances in Kernel Methods - Support Vector Learning*, 1999.

[11] N. Chronis and L. Lee, "Electrothermally activated su-8 microgripper for single cell manipulation in solution," *Journal of Microelectromechanical Systems*, vol. 14, no. 4, pp. 857–863, Aug 2005.

[12] J. Desai, A. Pillarisetti, and A. Brooks, "Engineering approaches to biomanipulation," *Annual Review of Biomedical Engineering*, vol. 9, pp. 35–53, Mar 2007.

[13] H. Huang, D. Sun, J. Mills, and W. Li, "Visual-based impedance force control of three-dimensional cell injection system," in *International Conference on Robotics and Automation (ICRA)*. IEEE, Apr 2007, pp. 4196–4201.

[14] X. Liu, Y. Sun, W. Wang, and B. Lansdorp, "Vision-based cellular force measurement using an elastic microfabricated device," *Journal of Micromechanics and Microengineering*, vol. 17, no. 7, pp. 1281–1288, Jul 2007.

[15] A. Pillarisetti, M. Pekarev, A. Brooks, and J. Desai, "Evaluating the role of force feedback for biomanipulation tasks," in *14th Symposium on Haptic Interfaces for Virtual Environment and Teleoperator Systems*. IEEE, Mar 2006, pp. 11–18.

[16] Z. Lu, P. Chen, R. Nam, J. Ge, and W. Lin, "A micromanipulation system with dynamic force-feedback for automatic batch microinjection," *Journal of Micromechanics and Microengineering*, vol. 17, no. 2, pp. 314–321, Feb 2007.

[17] Y. Sun, K.-T. Wan, K. Roberts, J. Bischof, and B. Nelson, "Mechanical property characterization of mouse zona pellucida," *Transactions on Nanobioscience*, vol. 2, no. 4, pp. 279–286, Dec 2003.

[18] X. Zhang, S. Zappe, R. Bernstein, O. Sahin, C.-C. Chen, M. Fish, M. Scott, and O. Solgaard, "Integrated optical diffractive micrograting-based injection force sensor," in *12th International Conference on Transducers, Solid-State Sensors, Actuators and Microsystems*, vol. 2. IEEE, 2003, pp. 1051–1054.

[19] S.-Y. Cho and J.-H. Shim, "A new micro biological cell injection system," in *IEEE/RSJ International Conference on Intelligent Robots and Systems (IROS)*. IEEE, Oct 2004, pp. 1642–1647.

[20] C. Stolle, "Distributed control architecture for automated nanohandling," in *International Conference on Informatics in Control, Automation and Robotics (ICINCO'07)*, 2007, pp. 127–132.